New theoretical infrared line list for the methyl radical with accurate vibrational band origins from high-level ab initio calculations

Oleg Egorov, Michael M. Rey, Andrei Nikitin, Dominika Viglaska

New theoretical infrared line list for the methyl radical with accurate vibrational band origins from high-level *ab initio* calculations

Oleg Egorov[1*], Michaël Rey[2], Andrei V. Nikitin[1], Dominika Viglaska[2]

[1]Laboratory of Theoretical Spectroscopy, V.E. Zuev Institute of Atmospheric Optics SB RAS 1, Akademician Zuev Sq., Tomsk, 634055 Russia

[2]Groupe de Spectrométrie Moléculaire et Atmosphérique UMR CNRS 7331, UFR Sciences BP 1039, 51687 Reims Cedex 2, France

Corresponding Author

*(O.E.) E-mail: oleg.egorov@iao.ru

ABSTRACT

In the present work, high-level *ab initio* calculations were carried out for the ground electronic state of the methyl radical (CH_3). The Dunning's augmented correlation-consistent orbital basis sets were employed up to the quintuple-ζ valence quality with the core-valence electron correlation [aug-cc-pCV5Z] combined with the single- and double-excitation unrestricted coupled cluster approach with a perturbative treatment of triple excitations [RHF-UCCSD(T)]. The explicitly-correlated version of the coupled cluster approach [RHF-UCCSD(T)-F12x{x=a, b}] was additionally applied with the core-valence cc-pCVQZ-F12 basis set in order to study convergence with respect to the basis set size. The contributions beyond the coupled cluster level of the theory like Douglas-Kroll-Hess scalar relativistic Hamiltonian, diabatic Born-Oppenheimer corrections and high-order electronic correlations have been included to the *ab initio* potential energy surfaces (PESs). It is shown that the theoretical band origins of CH_3 converge gradually to the experimental values when applying the *ab initio* PESs using the aug-cc-pCVXZ [X = T, Q, and 5] basis sets. For the first time, all available experimental band origins of the gaseous CH_3 are reproduced within an accuracy of 0.2 cm^{-1} using a newly developed PES extrapolated to the Complete Basis Set limit [CBS(TQ5Z)]. The reached accuracy is one order of magnitude better than that of the best available calculations. A new theoretical infrared line list was generated for astrophysical applications using an *ab initio* dipole moment surface computed at the RHF-UCCSD(T)/aug-cc-pCVQZ level of the theory. The manifestation of a large amplitude motion in CH_3 is also discussed.

Keywords: CH_3, *ab initio*, potential energy surface, dipole moment surface, band origins, line list, large-amplitude motion

1. INTRODUCTION

Methyl radical (CH_3) is an intermediate species in chemical reactions associated with the production and destruction of the complex hydrocarbons, precursor in the formation of the carbon films during the chemical vapor deposition (see e.g. refs 1–4). Due to its very high reactivity, the CH_3 lifetime cannot be long under the Earth's conditions but it increases in rarefied gaseous media which is typical for astronomical objects. There are essentially two natural ways to form CH_3. The first one is based on the photolysis of methane, namely $CH_4 + h\nu \rightarrow CH_3 + H$ that can occur in planetary atmospheres.[5–7] The second one is based on a series of ion-molecular reactions in the cold low-density interstellar medium $CH_x^+ + H_2 \rightarrow CH_{x+1}^+ + H$, where the reaction $C + H_3^+ \rightarrow CH^+ + H_2$ initiates the formation of the C–H bonds.[8] Note that ethane, which is the second strongest abundant hydrocarbon in the atmospheres after CH_4, can be formed via the reaction: $2CH_3 \rightarrow C_2H_6$. So far, CH_3 was detected by the Infrared Space Observatory in Saturn,[9] Neptune,[10] and in the interstellar medium toward the Sagittarius A* radio source.[11]

The present work aims at first computing an accurate PES for CH_3 using advanced *ab initio* calculations before constructing a comprehensive, room-temperature line list from variational calculations. The previously published works (see e.g. refs 12–15) were based on both the multireference configuration interaction method and the explicitly correlated coupled cluster approach but they were not able to accurately reproduce the observed energy levels. For example, in the last study by Adam *et al.*[15] the errors on the band centers were of 4 and 9 cm^{-1} for ν_2 and $2\nu_2$, respectively. Such deviations are surprisingly big if we keep in mind that the ground electronic state of CH_3 is quite well isolated from the first excited state located at 216 nm or ~ 46000 cm^{-1}. This paper is a continuation of our previous studies focused on the construction of theoretical line lists of rigid and non-rigid polyatomic molecules of different symmetries from accurate *ab initio* potential energy (PESs) and dipole moment surfaces (DMSs). It is structured as follows. First, the state-of-the-art in the CH_3 spectroscopy is given in Section 2. The construction of the PES and DMS will be reported in Section 3. The final results including the corrections due to advanced *ab initio* methods and high order electronic correlation effects will be discussed in Section 4 before concluding in Section 5.

The *ab initio* calculations reported in this work were performed by using the MOLPRO,[16,17] MRCC,[18,19] and CFOUR[20,21] packages while the nuclear motion calculations were carried out from our home-made variational computer code TENSOR[22–24] applied with success in refs 25–34 for computing accurate spectroscopic line lists of semirigid molecules. As in ref 35, a hybrid nonrigid Hamiltonian model was built in this work using the Hougen−Bunker−Johns formalism[36] where the relation between the curvilinear $\bar{\rho}$ and effective coordinates ρ was explicitly established in ref 37.

2. STATE-OF-THE-ART IN THE CH_3 SPECTROSCOPY

CH_3 has one unpaired electron, therefore its ground electronic state (denoted to as $\tilde{X}\,^2A_2''$ in the D_{3h} point group) is a doublet state. Consequently, the vibration-rotation spectra should exhibit spin-rotation splittings. Due to its planar configuration at the equilibrium geometry in the $\tilde{X}\,^2A_2''$ state, CH_3 has no permanent dipole moment and consequently exhibits only weak magnetic-dipole rotational transitions (see ref 38 and reference therein for further details).

Early experimental studies by Herzberg and Shoosmith[39,40] were devoted to the ultraviolet absorption spectrum where the band at 216 nm (and 214.5 nm for CD_3) was observed. This band obeys Rydberg formula and corresponds to the excitation of the unpaired electron located on the molecular $2p_z$ character orbital into the 3s one. The structure and dissociation dynamics of the vibronic levels of the 3s Rydberg state ($\tilde{B}\,^2A_1$) which is the lowest excited electronic state of CH_3 (D_{3h}) were further studied in refs 41–45. The vibrational feature at 212.7 nm observed by Callear *et al.*[41] was assigned to the hot band $\tilde{B}\,^2A_1(0100) \leftarrow \tilde{X}\,^2A_2''(0100)$ by Westre *et al.*[43] This hot band was detected at 211.6 nm for CD_3. Another absorption at 207 nm was assigned to the cold band $\tilde{B}\,^2A_1(1000) \leftarrow \tilde{X}\,^2A_2''(0000)$ from analysis of the resonance Raman spectrum.[43] At higher energies, in particular at 193 nm, a broad continuum was observed due to the photodissociation of CH_3.[46] Note that the energies of the Rydberg states correlate with the excited electronic states of methylene (CH_2) in the dissociation channel $CH_2(C_{2v}) + H(^2S)$ which leads to the strong predissociation properties.[47–49] In particular, for the 3s Rydberg state the empirical and theoretical values of the barrier estimated in refs 42 and 50 were of 6.29 kcal/mol (~2200 cm^{-1}) and 2417 cm^{-1}, respectively for the reaction: $CH_3(\tilde{B}\,^2A_1) \rightarrow CH_2(\tilde{a}\,^1A_1) + H(^2S)$, where $\tilde{a}\,^1A_1$ is the first excited singlet electronic state of CH_2.

Next electronic transitions in CH_3 are associated with the $3p_{xy}$ ($^2E'$) and $3p_z$ ($^2A_2''$) Rydberg states. The energy of the $3p_{xy}(^2E') \leftarrow \tilde{X}\,^2A_2''$ vertical excitation calculated in refs 48, 51 and 52 varied within 6.95–7.17 eV (172.9–178.4 nm). The $3p_z(^2A_2'') \leftarrow \tilde{X}\,^2A_2''$ band was measured by the Resonance-Enhanced Multiphoton Ionization (REMPI) spectroscopy in refs 53–61. Simultaneous absorption of two photons with energies between 325 and 336 nm resulted in the detection of several absorptions with the maximum located at 333.4 nm that is about 166.7 nm (59972 cm^{-1}) in terms of two-photon energy. The frequency of the ν_2 mode at the $3p_z(^2A_2'')$ Rydberg state extracted in refs 55, 57 and 61 was about two times bigger when comparing with the ground electronic state whereas other fundamentals, particularly ν_1[57,61] and ν_3[58] were red-shifted by ~74 cm^{-1}. Some of the higher excited Rydberg states (4p, 4f, and 5f) were also detected by the REMPI spectroscopy in refs 55, 62 and 63.

As to the infrared spectra, the region of the out-of-plane bending vibration (ν_2 band) associated with the strongest *z* component of the molecular dipole of CH_3 and located at 606 cm^{-1} (or 16.50 μm) was one of the first for which high-resolution studies were carried out. In early works,[64–66] the spectra of CH_3 were recorded by the matrix isolation technique with a certain shift in the frequency depending on the inert gas matrix applied (argon, nitrogen, neon etc.). Tan *et al.*[67] recorded the spectra of the gaseous short-lived CH_3 with the help of the rapid-scanning infrared spectrometer. Yamada *et al.*[68] applied the pyrolysis and electric discharge approaches to produce CH_3 and used a diode laser spectrometer. As a result, the rotational structures of the ν_2, $2\nu_2–\nu_2$ and $3\nu_2–2\nu_2$ bands were resolved in the gas phase. The spin-rotation parameters extracted from the observed spin-rotational splitting were in a good agreement with the theoretical estimation.

Although the ν_1 symmetric stretch band of CH_3 is not infrared active, its rotational structure (especially, *Q*-branch) was explicitly resolved at 3004 cm^{-1} by the Coherent anti-Stokes Raman Spectroscopy (CARS) in refs 69–71 using the second harmonic of the YAG laser as a pumping beam and by the resonance Raman spectroscopy in ref 72. The spectra obtained in ref 71 under the near-nascent conditions show the domination of the ground vibrational state of CH_3 when it is produced by the UV laser photolysis from CH_3I. This agrees with the theoretical study[73] which predicts a slow relaxation from the pyramidal to the planar configurations after the bond breaking.

The *x* component of the molecular dipole is responsible for the infrared absorption in the regions of the ν_3 and ν_4 bands (in-plane degenerate asymmetric stretch and bend, respectively). The difference frequency laser spectrometer applied in ref 74 allowed to record several series of the *Q*-branch transitions of the ν_3 band located at 3161 cm^{-1}. The absorption of this band was then remeasured in ref 75 under the sub-Doppler conditions that allowed to resolve the spin-rotation and partially nuclear hyperfine splitting. To our knowledge, there is no studies of the ν_4 band of the gaseous CH_3 to confirm results of the matrix isolation spectroscopy: its band origin varies from 1385 to 1403 cm^{-1}, depending on the gas matrix (see e.g. refs 65, 76–78).

When extracting the line intensities of CH_3 from the measured spectra, the most complicated issue is the determination of the concentration and temperature inside the cell under the plasma conditions. Currently, the vibrational transition moments ($\mu_{V''}^{V'}$) of three infrared bands, namely, ν_2, $2\nu_2–\nu_2$, and ν_3 were analyzed at different levels of accuracy. In early works,[79,80] the peak absorbances of the single transition belonging to the *Q*-branch of ν_2 was measured to calculate its $\mu_{V''}^{V'}$. Stancu *et al.*[81] examined the line intensities of ten transitions of the ν_2 band by including line profiles to determine accurately the temperature. The obtained value of $\mu_{V''}^{V'}$ was in a good agreement with the *ab initio* estimations, particularly, with ref 82. According to refs 83–85, the ν_3 band is about 6.5 times

weaker than v_2 in terms of $\mu_{V''}^{V'}$, whereas for the hot band $2v_2–v_2$ the $\mu_{V''}^{V'}$ value is about 1.5 times stronger.[86]

Note that the $\mu_{V''}^{V'}$ values in experimental works were determined at the zero-order approximation i.e. without rotation-vibration couplings. Such approach can provide satisfactory results for the strongest bands (e.g. for v_2 of CH_3) but turns out not sufficient to predict weaker bands whose intensities mainly come from vibrational-rotational interactions. A new, non-perturbative approach was recently proposed in ref 87 to obtain the transition moment spectroscopic effective parameters directly from the *ab initio* DMS for computing both cold and hot bands.

3. CONSTRUCTION OF THE PES AND DMS

3.1. Analytical representation. The PES and DMS of CH_3 are both expressed in this work as a Taylor power series expansion in terms of symmetry coordinates S_i. This analytical representation, which converges quite rapidly despite the out-of-plane bending vibration, has been recently used to describe the NH_3 PES with its 2 minima separated by a barrier of 2000 cm^{-1}.[35] The D_{3h} symmetry coordinates associated with the symmetric and asymmetric stretching and in-plane bending vibrations are defined using the projection technique[88] as follows

$$\begin{cases} S_1^{A_1'} = (y_1 + y_2 + y_3)/\sqrt{3} \\ S_{3a}^{E'} = (2y_1 - y_2 - y_3)/\sqrt{6} \\ S_{3b}^{E'} = (y_2 - y_3)/\sqrt{2} \\ S_{4a}^{E'} = (2\varphi_1 - \varphi_2 - \varphi_3)/\sqrt{6} \\ S_{4b}^{E'} = (\varphi_2 - \varphi_3)/\sqrt{2} \end{cases} \quad (1)$$

where y_k and φ_k with k = 1, 2, and 3 are functions depending on the internal coordinates. Here, we have considered the Morse-type functions

$$y_k = 1 - \exp\left[-b\cdot(r_k - r_e)\right], \quad (2)$$

for the stretching part with b = 1.9 $Å^{-1}$ and the cosine functions

$$\varphi_k = \cos(\alpha_k) - \cos(\alpha_e), \quad (3)$$

for the bending part.

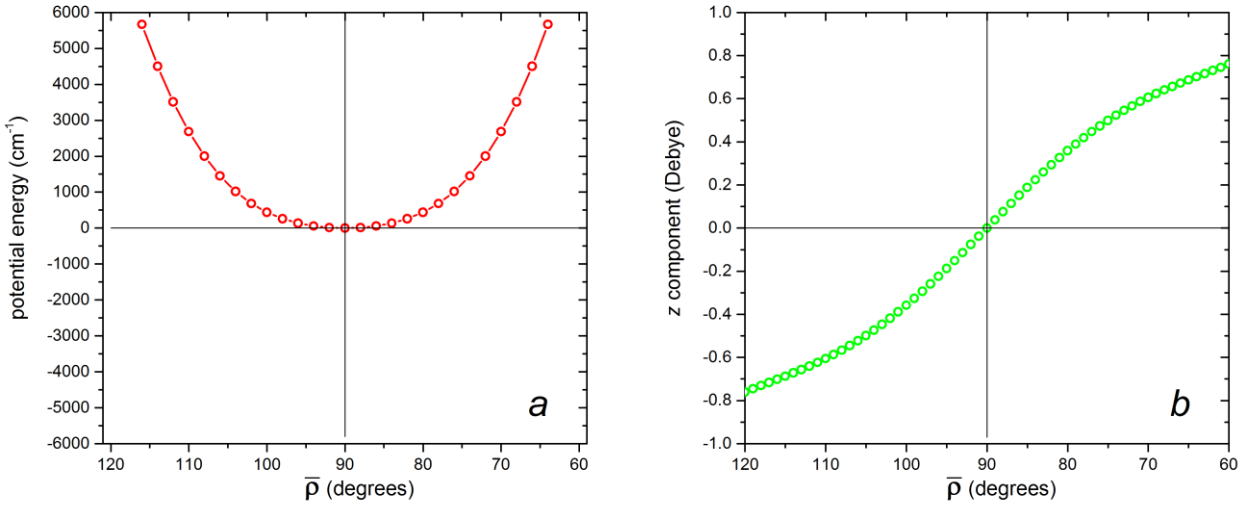

Figure 1. Behavior of the potential energy (*a*) and *z* component of the dipole (*b*) of CH_3 along the out-of-plane bending angle (calculations were made at the RHF-UCCSD(T)/ACVQZ level; all non-scanned coordinates were fixed to their equilibrium values).

Note that Eqs. (1–3) are the same for both the PES and DMS while the out-of-plane bending coordinate is different. Indeed, the sign of the *z* component of the dipole between 0° to 90° and between 180° to 90° is different whereas it is the same for the PES (see Figure 1). Consequently, a sine function

$$S_2^{A_1'} = \sin(\rho_e) - \sin(\bar{\rho}) \tag{4}$$

will be used for the PES (here $\rho_e \equiv \bar{\rho}_e$, see ref 37) and a cosine function

$$S_2^{A_2''} = \cos(\bar{\rho}) \tag{5}$$

for the DMS, where $\bar{\rho}$ can be related to the three in-plane bending angles as follows

$$\bar{\rho} = \arcsin\left(\frac{2}{\sqrt{3}}\sin\left[(\alpha_1+\alpha_2+\alpha_3)/6\right]\right). \tag{6}$$

The use of symmetry coordinates which transform as the irreducible representations of the molecular symmetry or point group[88,89] allows to express the PES or DMS as sum-of-products of irreducible tensor operators $\boldsymbol{R}_j^p$

$$V\left(S_1^{A_1'}, S_2^{A_1'}, S_{3a}^{E'}, S_{3b}^{E'}, S_{4a}^{E'}, S_{4b}^{E'}\right) = \sum_{p=0}^{p_{\max}} \sum_j C_j \cdot \boldsymbol{R}_j^p \tag{7}$$

where C_j are expansion coefficients to be determined and the irreducible tensors are written as

$$\boldsymbol{R}_j^p = \sum_{i=1}^{n} T_i \cdot \left[S_1^{A_1'}\right]^{p_i^1} \cdot \left[S_2^{A_1'}\right]^{p_i^2} \cdot \left[S_{3a}^{E'}\right]^{p_i^3} \cdot \left[S_{3b}^{E'}\right]^{p_i^4} \cdot \left[S_{4a}^{E'}\right]^{p_i^5} \cdot \left[S_{4b}^{E'}\right]^{p_i^6}. \tag{8}$$

The T_i 's are computed from the D_{3h} Clebsch-Gordan coupling coefficients and each term in Eq. (8) is of order *p*. The tensor formalism used in this work shares the same coupling coefficients and phase factor conventions with the variational computer code TENSOR. Since the PES is totally symmetric, Eq. (7) must contain only the terms which transform as A_1'. The dipole moment operator has a similar expansion, except its *z* and (*x*,*y*) components will transform as A_2'' and E', respectively.

3.2. *Ab initio* calculations. In order to study the ground electronic state of the open-shell CH_3 radical, the spin-unrestricted coupled cluster (CC) method [RHF-UCCSD(T)] implemented in MOLPRO by Knowles *et al.*[90,91] was employed. The unpaired electron was located on the $2p_z$ molecular orbital during all calculations that corresponds to the $\tilde{X}\,^2A_2''$ state of CH_3. The pragmatic CC approach provides accurate and size-consistent calculations of the correlation energy especially for single-reference electronic states. To estimate the multireference character of the $\tilde{X}\,^2A_2''$ state, the T1 and D1 diagnostic numbers were extracted from the output files of MOLPRO. As depicted in Figure 2, we can see that the maximum values of T1 and D1 are about two times less than their critical values of 0.02 and 0.05, respectively, established in refs 92 and 93 for all the nuclear configurations of the grid.

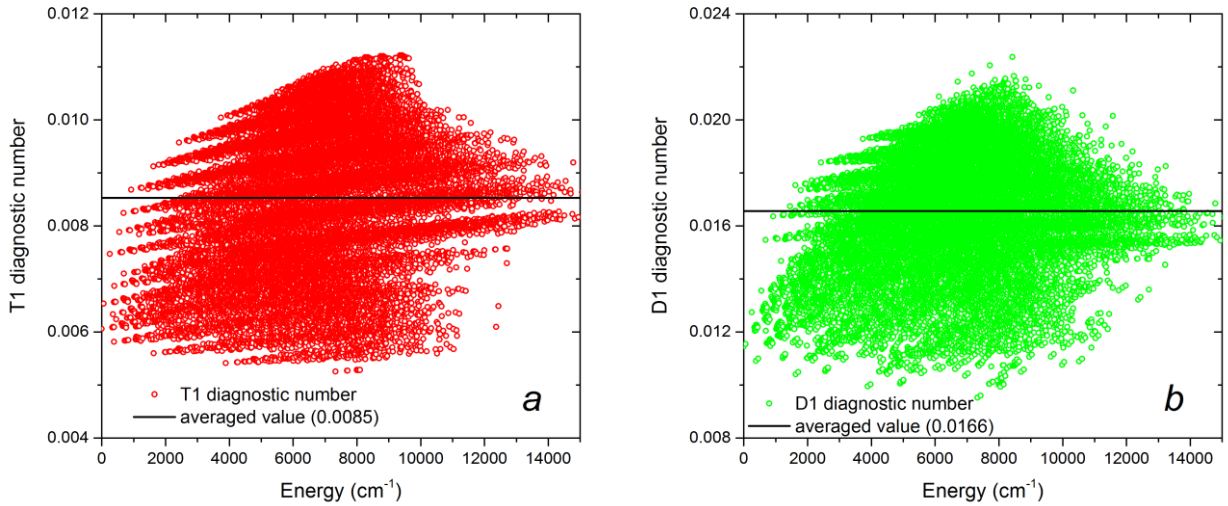

Figure 2. T1 (*a*) and D1 (*b*) diagnostic numbers for the $\tilde{X}\,^2A_2''$ state of CH_3 produced by MOLPRO when calculating the potential energy at the RHF-UCCSD(T)/ACVQZ level of the theory for "Grid_1" composed of 36032 nuclear configurations (for more details, see section 3.3). Note that the averaged T1 and D1 values are one third of their critical values of 0.02[92] and 0.05,[93] respectively.

Contrary to previous *ab initio* studies, in particular refs 12 and 13, the Dunning's *aug*mented correlation-consistent orbital basis sets[94] were applied up to the quintuple-ζ valence quality with the

core-valence electron correlation [aug-cc-pCV5Z, hereafter, ACV5Z]. In the case of the correlation-consistent basis set, the *ab initio* energies can be further extrapolated to the Complete Basis Set (CBS) limit using different extrapolation formula.[95] In this work, we used the three-point exponential functional

$$E_X^{total} = E_{CBS}^{total} + A \cdot \exp(-C \cdot X) \quad (9)$$

which was recently applied with success in ref 35 for NH_3. In Eq. (9) E_X^{total} and E_{CBS}^{total} are the total energies (Hartree-Fock (reference) + correlation) corresponding to the ACVXZ (X = T, Q, and 5) basis set and CBS limit, respectively.

Along with the "standard" CC method, the simplified explicitly correlated versions [RHF-UCCSD(T)-F12x{x=a, b}] of Knizia *et al.*[96] were also employed in order to reach the CBS limit without extrapolation. According to refs 35 and 97, the accuracy of the F12b method combined with the correlation-consistent core-valence cc-pCVQZ-F12 basis set (hereafter, CVQZ-F12) is comparable to that of the sextuple-ζ basis set.

In the CBS limit, further corrections beyond the CC level of the theory are required to predict the band centers within 1 cm^{-1} or below of accuracy. There are three types of corrections that are actually analyzed when considering the ground electronic state: scalar relativistic effects (relativistic), diabatic Born-Oppenheimer correction (DBOC), and contributions to the correlation energy from the highly-excited Slater determinants. Since the convergence of the high-order CC methods is quite fast with respect to the basis set size, the cc-pVTZ basis set will be enough to completely include the contributions from the triple [CCSDT] and quadruple [CCSDT(Q)] excitations whereas the cc-pVDZ basis set will be used for the pentuple excitations. Note that the MRCC and CFOUR packages consider the unrestricted Hartree-Fock (UHF) reference wave function, making the open-shell CC method different to that implemented in MOLPRO. For this reason, the *ab initio* energies computed from MOLPRO were not used when making the scaling from CCSD(T) to CCSDT. All the energy differences, namely [CCSDT–CCSD(T)]/cc-pVTZ, [CCSDT(Q)–CCSDT]/cc-pVTZ, and [CCSDT(Q)–CCSDTQP]/cc-pVDZ were calculated using the *ab initio* energies from MRCC.

The relativistic correction was calculated using the Douglas-Kroll-Hess (DKH) scalar relativistic Hamiltonian available in MOLPRO. A fourth order DKH Hamiltonian was combined with the ACVTZ-DK basis set. The energy contributions from higher order transformations were found to be less than 10^{-4} cm^{-1}. The DBOC correction was calculated at the UHF-CCSD/cc-pVTZ level in CFOUR. According to extensive benchmarks from ref 98, "…the CCSD approach is a good choice for the accurate calculation of the DBOC…" because it provides the contribution of about 90 % to the electron correlation energy.

As to the *ab initio* dipole moment, it was calculated *via* the finite difference approximation as the first derivative of the potential energy with respect to the electric field. Since CH_3 is a symmetric top molecule, only two components of the dipole moment were necessary. Here, a field was applied along the *x* and *z* axes with the magnitudes of 0.002 a.u. and –0.002 a.u. The RHF-UCCSD(T)/ACVQZ method was applied for the energy calculations.

3.3. Definition of the two grids for the nuclear configurations. Because of the high-quality but costly basis sets and corrections beyond the RHF-UCCSD(T) level employed in this work to construct the PES, two different grids of nuclear configurations have been considered. A similar strategy was already applied for other molecules (see e.g. CH_4,[99] H_2CO,[100] and NH_3[35]).

The first grid (called Grid_1) was generated by varying simultaneously all the six coordinates defined by Eqs. (1) and (6). The $\bar{\rho}$ coordinate takes the following values (here in degrees): 90, 94, 98, 102, 106, 108, 110, and 112. The two components $S_{3b}^{E'}$ and $S_{4b}^{E'}$ of the stretching and bending coordinates take values between 0 to 0.20 and between 0 to 0.72, respectively, while the ranges for $S_1^{A_1'}$, $S_{3a}^{E'}$ and $S_{4a}^{E'}$ are the following: [–0.2, 0.25], [–0.2, 0.25], and [–0.72, 0.90], respectively. Finally, the Grid_1, which is composed of 36032 nuclear configurations up to 15000 cm^{-1}, was used to compute (i) the PES at the RHF-UCCSD(T)/ACVQZ and RHF-UCCSD(T)-F12x{x=a,b}/CVQZ-F12 levels and (ii) the *x* and *z* components of the DMS at the RHF-UCCSD(T)/ACVQZ level. This Grid_1 was fitted with a Root Mean Square (RMS) deviation of 0.18 cm^{-1} for the PES and of 0.000627 (resp. 0.00038) Debye for the *z* (resp. *x*) component of the DMS using 303 and 61 (resp. 143) expansion coefficients in Eq. (7). The fitted sets of the parameters included the irreducible tensor operators up to 8th and 6th orders for the PES and DMS, respectively.

The second grid (called Grid_2) was generated using totally symmetric (A_1') irreducible tensors up to order 8 and is composed of 5849 points for the PES up to 10000 cm^{-1}. The Grid_2 was used to calculate the energies at the RHF-UCCSD(T)/ACVXZ (X=T, Q, and 5) levels as well as all corrections that are quite demanding (see section 3.2). As in refs 35 and 99, the energy differences, namely, RHF-UCCSD(T)/[ACVTZ-ACVQZ], RHF-UCCSD(T)/[ACV5Z-ACVQZ], and RHF-UCCSD(T)/[CBS(TQ5Z)-ACVQZ] have a smooth behavior and were fitted with an RMS error less than 0.1 cm^{-1}. The predicted energy differences were then used to correct the energies RHF-UCCSD(T)/ACVQZ calculated for the whole Grid_1 in order to obtain extrapolated ACVTZ, ACV5Z, and CBS(TQ5Z) PESs. The same strategy was employed to include the sum of the five corrections (relativistic + DBOC + CCSDT + CCSDT(Q) + CCSDTQP) fitted with an RMS error of 0.045 cm^{-1} to the whole Grid_1.

4. RESULTS AND DISCUSSION

4.1. Equilibrium geometry and vibrational band origins. The equilibrium geometry (r_e) of CH_3 was obtained as the stationary point of the fitted PES and allowed us to analyze the contributions of various corrections to r_e. According to Table 1, there is a good agreement (error of 0.00006 Ang.) between the results at the CBS(TQ5Z) limit and those provided by the explicitly correlated F12x{x=a, b} methods. Through a series of corrections, the equilibrium geometry became closer to the value r_e = 1.076298 Ang. obtained in ref 15 from an empirical optimization of the *ab initio* PES. It is necessary to stress, however, that our theoretical r_e cannot be directly compared to the experimental data derived from the rotational constants because the ground vibrational state lies higher (by Zero-Point-Energy) than the global minimum of the PES. Our *ab initio* A=B=9.5820 cm^{-1} and C=4.7396 cm^{-1} rotational constants of the ground vibrational state agree within 0.0041 cm^{-1} and 0.0024 cm^{-1} with the empirical values from ref 68.

Table 1. Equilibrium geometry (r_e in Ang.) of CH_3 (D_{3h}) at the RHF-UCCSD(T) level of the theory and after adding various corrections[a]

Basis	RHF–UCCSD(T)	+Rel.	+DBOC	+CCSDT	+CCSDT(Q)	+CCSDTQP
ACVTZ	1.078220	1.078103	1.078243	1.078394	1.078458	1.078465
ACVQZ	1.076552	1.076433	1.076574	1.076723	1.076787	1.076794
ACV5Z	1.076025	1.075907	1.076047	1.076196	1.076259	1.076266
CBS(TQ5Z)	1.075788	1.075670	1.075810	1.075958	1.076022	1.076029
–F12a/CVQZ-F12	1.075849	1.075731	1.075872	1.076020	1.076083	1.076090
–F12b/CVQZ-F12	1.075842	1.075724	1.075865	1.076013	1.076076	1.076083

[a]Details of the calculation can be found in section 3.2.

All geometries were obtained from the fitted PESs.

The biggest contribution to r_e of 0.000148 Ang. was obtained using the CCSDT correction. The contributions from CCSDT(Q) and CCSDTQP of 0.000063 Ang. and 0.000007 Ang. clearly indicate the negligible effect of the higher excited determinants (e.g. sextuple order) to the correlation energy of CH_3. We also tested the convergence of the highly-correlated CC methods with respect to the basis set size. The (T)→T scaling using the lower level cc-pVDZ basis set resulted in a difference of +0.000055 Ang. in r_e compared to the cc-pVTZ one. On the other hand, the scaling from T to (Q) gave the same contribution to r_e when using the cc-pVDZ and cc-pVTZ basis sets. This simple test confirms the fast convergence of the high-order CC methods with respect to the basis set size and gives the guaranty that the cc-pVDZ basis set is more than enough for the (Q)→P scaling. Currently, the CCSDTQP/cc-pVTZ calculations are too costly.

Table 2. Theoretical band origins of CH_3 predicted from the *ab initio* PESs constructed using different orbital basis sets[a]

Band					Exp.[b]	Exp.[b] – Calc.					
V_1	V_2	V_3	V_4	Γ_{vib}		ACVTZ	ACVQZ	ACV5Z	CBS(TQ5Z)	CVQZ-F12b	CVQZ-F12a
0	1	0	0	A_2''	606.4531(6)[c]	8.690	2.377	0.538	–0.223	0.575	–1.143
0	2	0	0	A_1'	1288.0900(10)[c]	14.772	4.156	1.086	–0.167	0.850	–1.757
0	3	0	0	A_2''	2019.1657(11)[c]	19.894	5.701	1.646	0.016	1.050	–2.181
1	0	0	0	A_1'	3004.436(12)[d, e]	9.065	3.704	1.265	–0.194	–0.046	0.094
0	0	1	0	E'	3160.82118(6)[f, h]	10.430	4.125	1.398	–0.202	–0.224	–0.170
Total RMS						**13.270**	**4.151**	**1.244**	**0.177**	**0.664**	**1.356**

[a]All our PESs were constructed using the RHF-UCCSD(T) and RHF-UCCSD(T)-F12x{x=a,b} methods with the basis set displayed in Table 2 and including the following corrections: relativistic, DBOC, and high-order electronic correlations [CCSDT, CCSDT(Q), and CCSDTQP]. The details can be found in section 3.2.

[b]Only gas-phase IR data are used for validation: *c* – Yamada *et al.*;[68] *d* and *e* – Triggs *et al.*[70] and Zahedi *et al.*;[71] *f* and *h* – Amano *et al.*[74] and Davis *et al.*[75]

For variational calculations the hybrid model implemented in our homemade computer code TENSOR was applied. The kinetic energy and potential parts were Taylor expanded in the five normal mode coordinates describing the `small' vibrations (associated here with the ν_1, ν_3, and ν_4 modes) for each point of a numerical grid of the nonrigid coordinate ρ describing the large amplitude motion (associated here with the ν_2 mode). To this end, the correspondence between the coordinate ρ involved in the kinetic energy operator of the Hougen-Bunker-Johns Hamiltonian[36] and the geometrically defined "real" coordinate $\bar{\rho}$ involved in the PES was made following ref 37. The final 10th order Hamiltonian included 11607 terms and was built on a grid of $\rho \in [0.41, 2.69]$ rad by step of 0.02. To achieve a convergence better than 0.01 cm^{-1} for the vibrational levels, the following numbers of basis functions were used: 7662, 6738, 14388, 5742, 6555, and 12276 for the symmetry blocks A_1', A_2', E', A_1'', A_2'', and E'', respectively. As in ref 35, the atomic masses were employed in the kinetic energy operator while the nuclear masses were used in the DBOC calculation, as it is implemented in the CFOUR code.

Our predicted band origins are displayed in Table 2 where no empirical corrections have been applied in this work. Table 2 shows that the calculated band origins of CH_3 converge gradually to the experimental values when going from the lowest [ACVTZ] to the highest [ACV5Z] basis sets. The less demanding explicitly correlated F12x{x=a, b} methods are good indicator of the convergence with respect to the basis set size. From the published benchmark calculations (see e.g. ref 96), it is known that the F12a method combined with the CVQZ-F12 basis set provides an overestimated

values of the correlation energy whereas the results based on the F12b method are comparable with the sextuple-ζ basis set. This is corroborated by our calculation: the frequency of the ν_2 band is 0.5 lower than the experimental value when using the F12b method and it is about 1 cm^{-1} bigger when the F12a method is applied. Therefore, the values of the converged vibrational energies with respect to the basis set size must fall between those provided by the F12a and F12b methods. In others words, they fall in the region of the sextuple-ζ basis set or slightly lower if we remember the approximate nature of the F12x{x=a, b} methods.

Although the ACV6Z basis set was not considered here because of its cost of calculation, the results based on the extrapolated to the complete basis set potential energies [RHF-UCCSD(T)/CBS(TQ5Z)] were enough to reproduce for the very first time all available experimental band origins of CH_3 with an RMS error of 0.177 cm^{-1}. Such deviation is close to that obtained from the weighted fit of the PES (0.183 cm^{-1}). Note that the accuracy of the faster method F12b/CVQZ-F12 is of 1 cm^{-1} which can be thus seen as a good alternative to the standard CC approaches for CH_3.

Table 3. *Ab initio* band origins of CH_3 calculated in this work in comparison with previous studies[a]

Band					Energy (cm^{-1})				Exp.[b]–Calc.			
V_1	V_2	V_3	V_4	Γ_{vib}	I	II	III	This work	I	II	III	This work
0	1	0	0	A_2''	596.32	591.70	602.43	606.68	10.13	14.75	4.02	–0.22
0	2	0	0	A_1'	1278.89	1266.20	1281.24	1288.26	9.20	21.89	6.85	–0.17
0	0	0	1	E'	1387.53	1388.39	1387.26	1390.66				
0	1	0	1	E''	1996.99	1991.79	2002.22	2008.63				
0	3	0	0	A_2''	2025.6	1994.20	2010.09	2019.15	–6.43	24.97	9.08	0.02
0	2	0	1	E'	2690.55	2673.95	2691.61	2700.01				
0	0	0	2	A_1'	2748.17	2750.70	2739.64	2756.82				
0	0	0	2	E'	2766.09	2767.81	2762.05	2773.08				
0	4	0	0	A_1'	2829.01	2763.20	2776.86	2787.63				
1	0	0	0	A_1'	2991.45	2988.50	3002.76	3004.63	12.99	15.94	1.68	–0.19
0	0	1	0	E'	3144.36	3142.62	3158.83	3161.02	16.46	18.21	1.99	–0.20
0	1	0	2	A_2''	3371.05	3367.10	3371.59	3386.62				
0	1	0	2	E''	3388.51	3382.97	3391.11	3402.09				
0	3	0	1	E''	3447.82	3407.54	3430.06	3440.16				
0	5	0	0	A_2''	3686.04	3557.70	3569.95	3581.61				
1	1	0	0	A_2''	3575.47	3572.80	3596.3	3603.44				
0	1	1	0	E''	3715.98	3710.21	3736.97	3743.45				

0	2	0	2	A_1'	–	4057.50	–	4088.06				
0	2	0	2	E'	–	4073.08	4091.72	4102.87				
0	0	0	3	E'	–	4107.74	4075.46	4115.54				
0	0	0	3	A_1'	–	4138.90	4120.58	4146.60				
0	0	0	3	A_2'	–	4138.00	–	4147.14				
0	4	0	1	E'	–	4179.66	–	4216.86				
1	2	0	0	A_1'	–	4234.30	4260.53	4269.70				
1	0	0	1	E'	–	–	–	4388.67				
0	2	1	0	E'	–	–	–	4405.25				
0	6	0	0	A_1'	–	–	4397	4411.42				
0	0	1	1	A_2'	–	–	–	4530.40				
0	0	1	1	E'	–	–	–	4535.01				
0	0	1	1	A_1'	–	–	4538.93	4544.87				
0	1	0	3	E''	–	–	4728.62	4756.68				
0	1	0	3	A_2''	–	–	4767.06	4785.99				
0	1	0	3	A_1''	–	–	–	4787.48				
0	3	0	2	A_2''	–	–	4822.79	4838.48				
0	3	0	2	E''	–	–	4839.85	4852.37				
1	1	0	1	E''	–	–	4983.16	4992.10				
1	3	0	0	A_2''	–	–	4981.52	4992.58				
0	5	0	1	E''	–	–	–	5025.67				
0	3	1	0	E''	–	–	–	5116.90				
0	1	1	1	A_1''	–	–	–	5124.28				
0	1	1	1	E''	–	–	–	5129.51				
0	1	1	1	A_2''	–	–	–	5139.35				
0	7	0	0	A_2''	–	–	–	5256.66				
0	0	0	4	A_1'	–	–	5364.56	5446.23				
0	0	0	4	E'	–	–	–	5460.52				
0	2	0	3	E'	–	–	–	5471.31				
0	2	0	3	A_1'	–	–	5480.07	5497.70				
0	2	0	3	A_2'	–	–	–	5498.32				
0	0	0	4	E'	–	–	–	5511.60				
0	4	0	2	A_1'	–	–	5607.2	5623.31				
				Total RMS					**11.56**	**19.52**	**5.52**	**0.18**

[a]First 50 levels are displayed. Total list up to 7000 cm^{-1} is given in Supporting Information I. This work PES has Zero-Point Energy of 6482.697 cm^{-1}.

[b]The sources of the experimental data are the same as in Table 2.

I – ic-MRCI(Q)/AVTZ by Schwenke;[12] II – ic-MRCI(Q)/AVTZ by Medvedev *et al.*;[13] III – RHF-RCCSD(T)-F12b/CVQZ-F12 by Adam *et al.*[15]

Since the RHF-UCCSD(T)/CBS(TQ5Z) PES provided the most accurate results, it was used for a comparison with the previous published studies. Our vibrational labels are the four vibrational quantum numbers as well as the vibrational symmetry in the D_{3h} point group. According to Table 3, the calculations based on the ic-MRCI(Q)/AVTZ PES from ref 12 are comparable with our results obtained at the RHF-UCCSD(T)/ACVTZ level (see Table 2). The best available band centers have been published in ref 15 using the partially spin restricted open-shell explicitly correlated CC method [RCCSD(T)-F12b/CVQZ-F12] and correspond to our RHF-UCCSD(T)/ACVQZ PES. According to the trial calculations in refs 90 and 91, the difference between RHF-UCCSD and RCCSD is generally smaller than the basis set error. To demonstrate this, a geometry optimization was performed for the ground $\tilde{X}\,^2A_2''$ state of CH_3 using the default settings in MOLPRO and the CVQZ-F12 basis set. The following r_e values (in Ang.) were obtained: 1.075829 and 1.075823 using RCCSD(T)-F12x{x=a,b}, and 1.075878 and 1.075874 using RHF-UCCSD(T)-F12x{x=a,b}. As it can be seen, the difference of 0.00005 Ang. is small and can be explained by the default energy threshold of 10^{-6} a.u. during the geometry optimizations in MOLPRO. Thus, we assume two main reasons why the predictions given in ref 15 are less accurate than expected. 1) the equilibrium geometry r_e=1.077369 Ang. used in ref 15 for the construction of the PES is not accurate enough and corresponds to a value obtained between ACVTZ and ACVQZ (see Table 1). 2) the corrections due to relativistic, DBOC, and high-order electronic correlation effects were not considered though they do not contribute significantly for the ν_2 and $2\nu_2$ bands (see Section 4.2).

4.2. Corrections beyond RHF-UCCSD(T). In this section, the contributions to the band origins of CH_3 obtained from various corrections are analyzed and discussed. Note that in Tables 2 and 3 all corrections have been already included to our PESs. It is also worth mentioning that according to Table 4 the various contributions on the CH_3 vibrational levels are closer to those of the CH_4 molecule than to those of NH_3 belonging to the same symmetry. Indeed, in NH_3,[35] the relativistic and DBOC corrections had big contributions (up to 9.3 cm^{-1} and –4.8 cm^{-1}, respectively) especially for the vibrational levels where ν_2 is involved. In CH_4,[99] on the contrary, their effects were within ±1 cm^{-1} for most of the vibrational bands whereas the high-order electronic correlations gave the main contribution.

Table 4. The contributions of the *ab initio* corrections beyond the RHF-UCCSD(T) level of the theory into band origins of CH_3[a]

Band					Relativistic	DBOC	CCSDT	CCSDT(Q)	CCSDTQP	Total
V_1	V_2	V_3	V_4	Γ_{vib}						
0	1	0	0	A_2''	–0.095	0.413	–0.472	0.184	0.064	0.093
0	2	0	0	A_1'	–0.091	0.686	–0.967	0.176	0.095	–0.101
0	0	0	1	E'	0.294	0.004	–0.750	–0.672	–0.059	–1.184
0	1	0	1	E''	0.188	0.407	–1.233	–0.498	0.003	–1.133
0	3	0	0	A_2''	–0.038	0.888	–1.484	0.076	0.112	–0.445
0	2	0	1	E'	0.184	0.678	–1.740	–0.517	0.033	–1.362
0	0	0	2	A_1'	0.548	0.030	–1.516	–1.324	–0.116	–2.379
0	0	0	2	E'	0.573	0.015	–1.507	–1.347	–0.119	–2.385
0	4	0	0	A_1'	0.053	1.024	–2.008	–0.062	0.117	–0.876
1	0	0	0	A_1'	–0.040	–0.485	–2.486	–1.125	–0.084	–4.221
0	0	1	0	E'	–0.068	–0.397	–2.485	–1.011	–0.101	–4.061
0	1	0	2	A_2''	0.430	0.408	–2.009	–1.161	–0.056	–2.388
0	1	0	2	E''	0.454	0.406	–2.003	–1.180	–0.057	–2.380
0	3	0	1	E''	0.232	0.883	–2.269	–0.629	0.047	–1.735
0	5	0	0	A_2''	0.085	0.897	–2.605	–0.004	0.095	–1.531
1	1	0	0	A_2''	–0.106	0.126	–2.900	–0.714	0.010	–3.584
0	1	1	0	E''	–0.201	0.018	–2.975	–0.800	–0.032	–3.989
0	2	0	2	A_1'	0.412	0.668	–2.535	–1.182	–0.026	–2.664
0	2	0	2	E'	0.452	0.650	–2.515	–1.239	–0.035	–2.687
0	0	0	3	E'	0.795	0.067	–2.287	–1.978	–0.172	–3.574
0	0	0	3	A_1'	0.836	0.033	–2.273	–2.021	–0.178	–3.603
0	0	0	3	A_2'	0.838	0.029	–2.272	–2.025	–0.179	–3.608
0	4	0	1	E'	0.310	1.038	–2.812	–0.693	0.052	–2.104
1	2	0	0	A_1'	–0.192	0.176	–3.469	–0.890	0.022	–4.354
1	0	0	1	E'	0.262	–0.461	–3.272	–1.849	–0.147	–5.467
0	2	1	0	E'	–0.218	0.283	–3.490	–0.806	0.000	–4.229
0	6	0	0	A_1'	0.267	1.041	–3.013	0.779	0.115	–0.810
0	0	1	1	A_2'	0.247	–0.331	–3.286	–1.740	–0.166	–5.276
0	0	1	1	E'	0.224	–0.385	–3.264	–1.702	–0.161	–5.289
0	0	1	1	A_1'	0.228	–0.403	–3.261	–1.720	–0.162	–5.318
0	1	0	3	E''	0.667	0.415	–2.789	–1.836	–0.115	–3.657

0	1	0	3	A_2''	0.700	0.409	–2.784	–1.860	–0.117	–3.651
0	1	0	3	A_1''	0.704	0.407	–2.782	–1.868	–0.118	–3.657
0	3	0	2	A_2''	0.443	0.870	–3.089	–1.281	–0.013	–3.071
0	3	0	2	E''	0.477	0.882	–3.072	–1.320	–0.016	–3.049
1	1	0	1	E''	–0.104	0.259	–3.715	–1.361	–0.068	–4.988
1	3	0	0	A_2''	0.089	0.120	–4.009	–1.173	0.038	–4.935
0	5	0	1	E''	0.393	1.033	–3.392	–0.536	0.040	–2.464
0	3	1	0	E''	–0.165	0.451	–4.016	–0.947	0.008	–4.669
0	1	1	1	A_1''	0.106	0.073	–3.780	–1.542	–0.098	–5.241
0	1	1	1	E''	0.059	0.055	–3.780	–1.448	–0.083	–5.197
0	1	1	1	A_2''	0.088	0.001	–3.756	–1.522	–0.095	–5.285
0	7	0	0	A_2''	0.377	0.710	–3.340	1.831	0.116	–0.307
0	0	0	4	A_1'	1.046	0.131	–3.083	–2.627	–0.238	–4.770
0	0	0	4	E'	0.943	0.251	–3.137	–2.451	–0.202	–4.596
0	2	0	3	E'	0.755	0.519	–3.266	–2.067	–0.124	–4.183
0	2	0	3	A_1'	0.681	0.664	–3.321	–1.910	–0.092	–3.977
0	2	0	3	A_2'	0.676	0.672	–3.325	–1.903	–0.091	–3.971
0	0	0	4	E'	1.085	0.062	–3.055	–2.689	–0.237	–4.834
0	4	0	2	A_1'	0.495	1.022	–3.670	–1.248	–0.006	–3.406

[a]First 50 levels are displayed. Total list up to 7000 cm^{-1} is given in Supporting Information I.

Given values are the differences in the band origins (in cm^{-1}) when the corresponding correction is taken into account. For example, the "DBOC" column means the difference in the band origins calculated at the [RHF-UCCSD(T)/CBS(TQ5Z)+Relativistic+DBOC] and [RHF-UCCSD(T)/CBS(TQ5Z)+Relativistic] levels of the theory

In the case of CH_3, the relativistic corrections give rather small contributions both for the stretching and out-of-plane bending vibrations and contribute more significantly on the bands where ν_4 is involved. Conversely, the contributions from DBOC is quite small for ν_4. In terms of absolute values, the relativistic and DBOC corrections were of 0.38 cm^{-1} and 0.45 cm^{-1} in average. As expected, the inclusion of the CCSDT correction resulted in the significant shifts (–2.73 cm^{-1} in average) for all band centers, in particular for the stretching vibrations. The last two corrections, namely CCSDT(Q) and CCSDTQP, gave contributions which gradually decrease: 1.27 cm^{-1} and 0.09 cm^{-1} in average, respectively. Finally, among the four fundamental vibrations, the sum of these corrections was the biggest for the ν_1 and ν_3 stretching bands (–4.221 cm^{-1} and –4.061 cm^{-1}, respectively) while we have a shift of –1.184 cm^{-1} for ν_4 and of 0.093 cm^{-1} for ν_2.

4.3. Large amplitude motion in CH_3. The choice of the irreducible representation for the S_2 symmetry coordinate has to be discussed. On the one hand, the CH_3 PES is symmetric with respect to the equilibrium configuration (contrary to the NH_3 molecule), therefore the out-of-plane bending vibration should obey the "standard" rules for the bending mode, namely $S_2\left(A_2''\right)=\cos\left(\bar{\rho}\right)$ (here $\cos\left(\rho_e=\pi/2\right)=0$) making allowed only even powers in the PES expansion and thus implying a quadratic shape near the equilibrium configuration.[12] This quadratic shape is crucial if, for example, the normal mode coordinates are used.

On the other hand, an anomalously large anharmonicity was revealed for the v_2 mode by Yamada *et al.*,[68] proving that the shape of the PES is not totally quadratic but quite flat instead, even for vibrations with small amplitudes. This feature was further examined by Hirota *et al.*,[101] who confirmed that higher order terms are needed in the PES for an accurate description of the v_2 mode because of the slow convergence of the normal mode series. According to ref 101, the out-of-plane bend strongly interacts with the A_1' symmetric stretch. In particular, the negative sign of the F_{122} anharmonic potential constant (defined in terms of the curvilinear coordinates) can be explained by the elongation of the C-H bonds when the out-of-plane angle is excited.

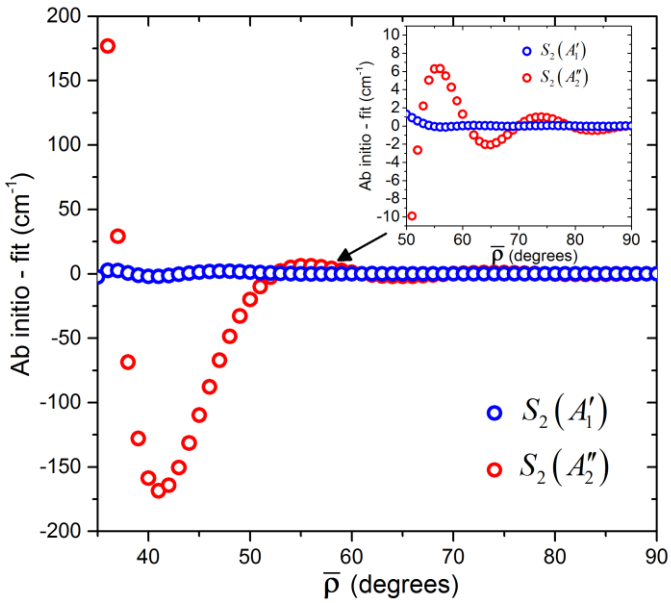

Figure 3. Fit of the *ab initio* 1D cut of the CH_3 PES along the out-of-plane bending angle. Blue and red scatters correspond to the fits based on the A_1' and A_2'' irreducible tensors operators up to the 8th order. The *ab initio* energies are calculated at the RHF-UCCSD(T)/ACVQZ level of the theory; all non-scanned coordinates were fixed to their equilibrium values.

In this work, the CH_3 PES was constructed by following the same approach as for NH_3 in ref 35. Both even and odd powers were allowed for the S_2 symmetry coordinate which transforms as the totally symmetric representation (see Eq. (4)). As expected, there is a strong linear term in the PES with a value of 0.10323 a.u associated with the S_2 coordinate. For NH_3 the linear terms were removed from the PES expansion after a geometry optimization. As an alternative, a fit using $S_2\left(A_2''\right)$ has been performed, leading to an RMS error of 0.54 cm^{-1} against 0.18 cm^{-1} when using $S_2\left(A_1'\right)$. The deviations of the fit of the 1D cut along the $\bar{\rho}$ coordinate are displayed in Figure 3. After several trials, the PES had to be expanded up to order 10 when using $S_2\left(A_2''\right)$ in order to obtain an RMS error similar to that when using $S_2\left(A_1'\right)$. Moreover, high order terms in the PES generally require computing additional points in the grid to obtain well-defined fitted high-order parameters. All the results presented in Tables 2-4 have been obtained using the new hybrid version of the TENSOR dealing with a large-amplitude coordinate.

4.4. New theoretical CH_3 line list in the infrared. The new *ab initio* PES and DMS presented in the previous section were used to generate the variationally-computed infrared line list of CH_3 that is compared below with the semi-empirical line list of Adam *et al.*[15] In this latter reference the *ab initio* DMS corresponds to the RCCSD(T)/AVTZ theoretical level of the theory. Here, "semi-empirical" means that the *ab initio* band origins of certain bands (namely, v_2, $2v_2$, v_1, v_4, and v_3) were replaced by the experimental values while the remaining bands are displayed in Table 3 in column "III".

Since the ground electronic state of CH_3 is a doublet there is a fine structure due to the spin-rotation coupling. According to ref 68, the spin-rotation splitting has the magnitude of 0.01 cm^{-1} that is lower than the expected accuracy of our theoretical line list. This was also corroborated in Tab. VII of ref 102. In this latter reference, the spin-rotation Hamiltonian was fitted as $H_{sr}=\left(-0.01183+0.351\cdot\cos^4\left(\rho\right)\right)\cdot N_y S_y$, where N_y and S_y are *y* components of the rovibronic and electron spin angular momenta, respectively.[88] In this work, the spin-rotation coupling term was not considered because of its quite weak contribution. Therefore, our spectral line positions are simply the transition frequencies between the vibration-rotation energy levels: $v_{fi}\left[\mathrm{cm^{-1}}\right]=E_f-E_i$.

The intensity of the spectral line [in cm^{-1} / (molecule·cm^{-2}) units] is calculated by the well-known expression (see e.g. ref 103):

$$I_{f\leftarrow i}=\frac{8\cdot\pi^3\cdot v_{fi}}{3\cdot h\cdot c\cdot Q(T)}\cdot g_i\cdot\exp\left(-\frac{E_i}{k_B T}\right)\cdot\left(1-\exp\left(-\frac{\tilde{\nu}_{fi}}{k_B T}\right)\right)\cdot S(f\leftarrow i) \qquad (10)$$

where the subscripts *f* and *i* refer to the *f*inal and *i*nitial (lower) states; $Q(T)$ is a partition function; g_i is a statistical weight of the lower state; E_i is the lower state energy; T is the temperature; $S(f \leftarrow i)$ is a line strength (the square of the matrix element of the molecular electric dipole moment); k_B is the Boltzmann constant (≈0.695031 $cm^{-1} \cdot K^{-1}$); h[erg·s] and c[cm/s] are the Planck constant and speed of light. The partition function is defined as a sum by all ro-vibrational states: $Q(T) = \sum_j g_j \exp(-E_j / k_B T)$. For CH_3, the statistical weights are given by 8, 0, 4, 8, 0, and 4 for the A_1', A_2', E', A_1'', A_2'', and E'' irreducible representations in the D_{3h} point group. Finally, the partition function calculated at T = 296 K is 715.96.

Table 5. Integrated intensities (S_v) of the strongest bands of CH_3 at T = 296 K[a]

Band	Origin (cm^{-1})	Range (cm^{-1})	S_v(cm / molecule)	Number of lines
$\nu_2(A_2'')$	606.676	151–989	$9.5288 \cdot 10^{-18}$	601
$\nu_2+\nu_4(E'')-\nu_4(E')$	617.969	235–1018	$2.1863 \cdot 10^{-20}$	1368
$2\nu_2(A_1')-\nu_2(A_2'')$	681.581	250–1238	$9.3576 \cdot 10^{-19}$	587
$3\nu_2(A_2'')-2\nu_2(A_1')$	730.893	333–1164	$4.8211 \cdot 10^{-20}$	561
$\nu_4(E')$	1390.665	844–1941	$8.8901 \cdot 10^{-19}$	1106
$\nu_2+\nu_4(E'')-\nu_2(A_2'')$	1401.958	892–2139	$5.1094 \cdot 10^{-20}$	1012
$3\nu_2(A_2'')$	2019.150	1340–2401	$1.0432 \cdot 10^{-20}$	506
$2\nu_2+\nu_4(E')$	2700.009	2223–3672	$2.7724 \cdot 10^{-20}$	1018
$2\nu_4(E')$	2773.080	2237–3719	$5.6534 \cdot 10^{-20}$	1386
$\nu_2+\nu_3(E'')-\nu_2(A_2'')$	3136.776	2548–3651	$1.2056 \cdot 10^{-19}$	1096
$\nu_3(E')$	3161.023	2513–3702	$1.7747 \cdot 10^{-18}$	1353
$\nu_1+\nu_2(A_2'')$	3603.443	3204–4710	$2.0471 \cdot 10^{-20}$	499
$3\nu_4(E')$	4115.543	3640–5242	$3.2020 \cdot 10^{-20}$	1091
$\nu_1+\nu_4(E')$	4388.674	3853–5150	$1.3373 \cdot 10^{-19}$	1102
$2\nu_2+\nu_3(E')$	4405.255	3865–5173	$1.4356 \cdot 10^{-20}$	1005
$\nu_2+\nu_3+\nu_4(E'')-\nu_2(A_2'')$	4522.834	4046–5040	$3.9800 \cdot 10^{-20}$	1197
$\nu_3+\nu_4(A_2')$	4530.401	3929–5271	$1.4535 \cdot 10^{-20}$	749
$\nu_3+\nu_4(E')$	4535.006	3950-5080	$9.1010 \cdot 10^{-19}$	1473
$\nu_3+\nu_4(A_1')$	4544.869	3991–5170	$1.2414 \cdot 10^{-20}$	721
$\nu_3+2\nu_4(E')$[b]	5882.889	5380–6608	$1.8948 \cdot 10^{-20}$	1895
$\nu_1+\nu_3(E')$	6080.087	5534–6617	$2.6499 \cdot 10^{-20}$	1009
$2\nu_3(E')$	6298.839	5588–6762	$6.3266 \cdot 10^{-20}$	1031

[a]All data were based on the developed *ab initio* line list. The integrated intensities are the sum of the intensities of the individual ro-vibrational lines of the certain band. The lines which intensities were bigger than 10^{-27} cm/molecule were included into the sum. The integrated intensities of the displayed bands are bigger than 10^{-20} cm/molecule.
[b]There is one more band centered at 5910.589 with the same vibrational assignment.

Our theoretical line list has been computed using the TENSOR computer code in the spectral range [0–7000] cm^{-1} up to $J = 20$ ($J \equiv N$, $S = 0$). The integrated intensities of the strongest cold and hot bands are displayed in Table 5. The absorbance spectra simulated at $P = 0.1$ Torr and $L = 20$ cm with a Gaussian profile and at resolution of 0.1 cm^{-1} are given in Figure 4. According to Table 5, there are three hot bands which fall in the region of the fundamental band $\nu_2(A_2'')$. Two bands, namely, $2\nu_2(A_1')$–$\nu_2(A_2'')$ and $3\nu_2(A_2'')$–$2\nu_2(A_1')$ were previously detected in ref 68. A part of absorption near the next two fundamental $\nu_4(E')$ and $\nu_3(E')$ bands is due to the relatively strong $\nu_2+\nu_4(E'')$–$\nu_2(A_2'')$ and $\nu_2+\nu_3(E'')$–$\nu_2(A_2'')$ hot bands. Above, the combination bands $\nu_1+\nu_4(E')$ and $\nu_3+\nu_4(E')$ are the strongest ones. The fundamental band $\nu_1(A_1')$ is not infrared active and is thus very weak.

Our *ab initio* line list is in good agreement, both for line positions and line intensities, with the semi-empirical list,[15] in particular in the spectral regions of $\nu_2(A_2'')$ and $\nu_3(E')$ (see Figures. 4*a* and 4*c*) where empirical corrections were applied. In the regions where no observation is available, the difference is much bigger. For example, the spectra in the $\nu_4(E')$ and $\nu_3+\nu_4(E')$ bands are shifted by +5 cm^{-1} and –6 cm^{-1} (see Figures 4*b* and 4*d*). It is also worth mentioning that our line intensities for $\nu_4(E')$ are two times stronger compared to those in ref 15. Our calculation is corroborated by the measurements of Snelson *et al.*[65] who obtained an intensity ratio of 10 between $\nu_2(A_2'')$ and $\nu_4(E')$ (see Table 5).

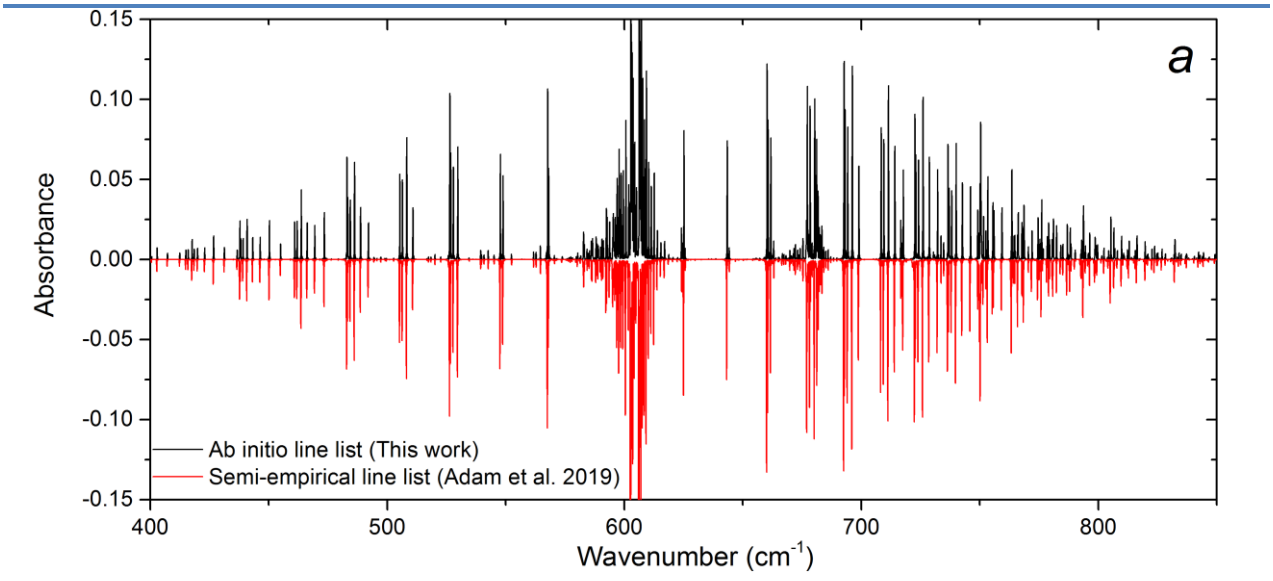

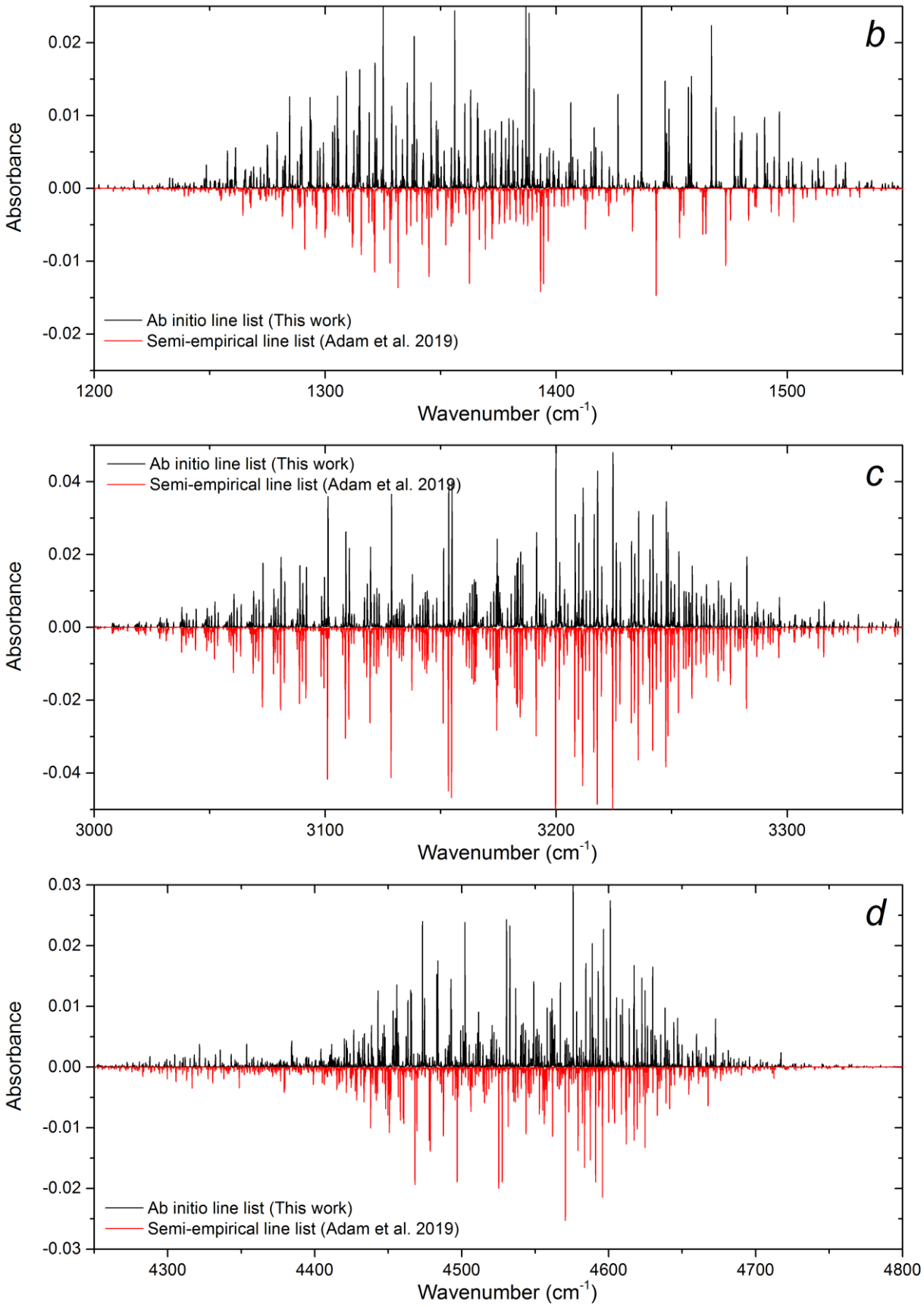

Figure 4. Absorbance of CH_3 simulated using the *ab initio* line list developed in this work compared to that based on the semi-empririal line list of Adam *et al.*[15] Labels *a*, *b*, *c*, and *d* correspond to the spectral regions of the following bands: *a*–$\nu_2(A_2'')$, *b*–$\nu_4(E')$, *c*–$\nu_3(E')$, and *d*–$\nu_3+\nu_4(E')$.

5. SUMMARY AND CONCLUSION

In this article, high-level *ab initio* calculations for CH_3 have been performed in order to reproduce the vibrational band centers of the ground electronic state within an accuracy of 1 cm^{-1}. The augmented correlation-consistent orbital basis sets were tested up to quintuple-ζ valence quality combined with the core-valence electron correlation [aug-cc-pCV5Z]. The quality of the calculated levels obtained from the "standard" open-shell coupled cluster approach [RHF-UCCSD(T)] was improved by including the following contributions: Douglas-Kroll-Hess scalar relativistic Hamiltonian, diabatic Born-Oppenheimer correction, and high-order electronic correlations. It has been thus demonstrated that the variationally computed band origins of CH_3 converge gradually to the experimental ones when applying the *ab initio* PESs using the aug-cc-pCVXZ [X = T, Q, and 5] basis sets. Finally, an RMS error of 0.18 cm^{-1} with respect to all the available experimental band origins of the gaseous CH_3 was obtained for the first time by extrapolating the *ab initio* potential energies to the Complete Basis Set limit [CBS(TQ5Z)]. Note that the reached accuracy is one order of magnitude better than that of the best available calculations. Another *ab initio* PES based on the less demanding explicitly correlated RHF-UCCSD(T)-F12b/cc-pCVQZ-F12 method allowed to predict the band origins with an RMS error of 0.66 cm^{-1}.

Among the fundamental vibrations, the corrections beyond the [RHF-UCCSD(T)] level of the theory had the biggest contributions for the stretching ones (up to –4.221 cm^{-1}) while the in-plane and out-of-plane bending vibrations have been corrected by –1.184 and 0.093 cm^{-1}, respectively. This work also confirmed the presence of the large-amplitude behavior for the out-of-plane ν_2 mode of CH_3. Since the $S_2\left(A_1'\right)$ linear term cannot be neglected, the shape of the PES is not totally quadratic near the equilibrium configuration making very limited the description of ν_2 in terms of the "standard" normal mode approach.

Our newly-developed *ab initio* PES was applied to calculate all the band centers falling in the region [0–7000] cm^{-1}. In this work, we report the most accurate theoretical values for the fundamental ν_4 band at 1390.66 cm^{-1} as well as for all other combination cold and hot bands with strong integrated intensities. The main advantage of using "pure" *ab initio* calculations for the construction of the line list has been clearly demonstrated when compared with the previously published empirically corrected line list.[15] Our theoretical line list is able to predict quite accurately spectral regions which were not studied so far. Undoubtedly, the results presented in this work will be useful for future high-resolution experimental studies of CH_3 as well as for astrophysical applications.

Our line list as well as the *ab initio* PESs and DMS are made available in Supporting Information.

Supporting Information

Supporting Information I, total list of the *ab initio* band origins of CH_3 calculated in this work up to 7000 cm^{-1} (Table S1); the effect of the *ab initio* corrections on the band origins of CH_3 (Table S2); Supporting Information II, the C++ code for computing potential energies and dipole moment from the constructed PESs and DMS; the *ab initio* line list of CH_3 with the complete quantum assignment up to 7000 cm^{-1} (ZIP); Supporting Information III, the *ab initio* points of the potential energies and dipole moment for the nuclear configurations of "Grid_1" and "Grid_2" calculated in this work (ZIP).

ACKNOWLEDGEMENTS

This work was supported by the joint "TEMMEX" project between the Russian Scientific Foundation (RSF, No. 22-42-09022) and Agence Nationale de la Recherche (ANR, French National Research Agency, Grant No. 21-CE30-0053-01). The support from the ROMEO computer center of Reims-Champagne-Ardenne as well as from the French–Russian collaboration program IRP SAMIA2 is also acknowledged.

REFERENCES

(1) Miller, J. A.; Kee, R. J.; Westbrook, C. K. Chemical Kinetics and Combustion Modeling. *Annu. Rev. Phys. Chem.* **1990**, *40*, 345–387.
(2) Fan, W. Y.; Röpcke, J.; Davies, P. B. Effect of oxygen on methyl radical concentrations in a CH_4/H_2 chemical vapor deposition reactor studied by infrared diode laser spectroscopy. *J. Vac. Sci. Technol. A.* **1996**, *14*, 2970.
(3) Scherer, J. J.; Aniolek, K. W.; Cernansky, N. P.; Rakestraw, D. J. Determination of methyl radical concentrations in a methane/air flame by infrared cavity ringdown laser absorption spectroscopy. *J. Chem. Phys*. **1997**, *107*, 6196.
(4) Tang, C. J.; Neves, A. J.; Fernandes, A. J. S. Study the effect of O_2 addition on hydrogen incorporation in CVD diamond. *Diamond and Related Materials*. **2004**, *13*, 203–208.
(5) Mordaunt, D. H.; Lambert, I. R.; Morley, G. P.; Ashfold, M. N. R.; Dixon, R. N.; Western, C. M.; Schnieder, L.; Welge, K. H. Primary product channels in the photodissociation of methane at 121.6 nm. *J. Chem. Phys*. **1993**, *98*, 2054.
(6) Gans, B.; Boyé-Péronne, S.; Broquier, M.; Delsaut, M.; Douin, S.; Fellows, C. E.; Halvick, P.; Loison, J. -C.; Lucchese, R. R.; Gauyacq, D. Photolysis of methane revisited at 121.6 nm and at 118.2 nm: quantum yields of the primary products, measured by mass spectrometry. *Phys. Chem. Chem. Phys*. **2011**, *13*, 8140–8152.
(7) Romanzin, C.; Arzoumanian, E.; Es-sebbar, Et.; Jolly, A.; Perrier, S.; Gazeau, M. -C.; Bénilan, Y. Combined experimental and theoretical studies on methane photolysis at 121.6 and 248 nm—implications on a program of laboratory simulations of Titan's atmosphere. *Planetary and Space Science*. **2010**, *58*, 1748–1757.
(8) Herbst, E.; Klemperer, W. The formation and depletion of molecules in dense interstellar clouds. *The Astrophysical Journal*. **1973**, *185*, 505–533.
(9) Bézard, B.; Feuchtgruber, H.; Moses, J. I.; Encrenaz, T. Detection of methyl radicals (CH_3) on Saturn. *Astron. Astrophys*. **1998**, *334*, L41–L44.
(10) Bézard, B.; Romani, P. N.; Feuchtgruber, H.; Encrenaz, T. Detection of the Methyl Radical on Neptune. *The Astrophysical Journal*. **1999**, *515*, 868–872.
(11) Feuchtgruber, H.; Helmich, F. P.; van Dishoeck, E. F.; Wright, C. M. Detection of Interstellar CH_3. *The Astrophysical Journal*. **2000**, *535*, L111–L114.
(12) Schwenke, D. W. A theoretical study of the ro-vibrational spectrum of the X state of CH_3. *Spectrochimica Acta Part A*. **1999**, *55*, 731–738.
(13) Medvedev, D. M.; Harding, L. B.; Gray, S. K. Methyl radical: ab initio global potential surface, vibrational levels and partition function. *Molecular Physics*. **2006**, *104*, 73–81.

(14) Adam, A. Y.; Yachmenev, A.; Yurchenko, S. N.; Jensen, P. Ro-Vibrational Averaging of the Isotropic Hyperfine Coupling Constant for the Methyl Radical. *J. Chem. Phys*. **2015**, *143*, 244306.
(15) Adam, A. Y.; Yachmenev, A.; Yurchenko, S. N.; Jensen, P. Variationally Computed IR Line List for the Methyl Radical CH_3. *J. Phys. Chem. A*. **2019**, *123*, 4755–4763.
(16) Werner, H. -J.; Knowles, P. J.; Manby, F. R.; Black, J. A.; Doll, K.; Heßelmann, A.; Kats, D.; Köhn, A.; Korona, T.; Kreplin, D. A.; Ma, Q.; Miller, T. F.; Mitrushchenkov, A.; Peterson, K. A.; Polyak, I.; Rauhut, G.; Sibaev, M. The Molpro quantum chemistry package. *J. Chem. Phys.* **2020**, *152*, 144107.
(17) Werner, H. -J.; Knowles, P. J.; Knizia, G.; Manby, F. R.; Schütz, M., et al. *MOLPRO*, version 2019.2, a package of ab initio programs, https://www.molpro.net (accessed July 6, 2022).
(18) Kállay, M.; Nagy, P. R.; Mester, D.; Rolik, Z.; Samu, G.; Csontos, J.; Csóka, J.; Szabó, P. B.; Gyevi-Nagy, L.; Hégely, B.; Ladjánszki, I.; Szegedy, L.; Ladóczki, B.; Petrov, K.; Farkas, M.; Mezei P. D.; Ganyecz, A. The MRCC program system: Accurate quantum chemistry from water to proteins. *J. Chem. Phys.* **2020**, *152*, 074107.
(19) Kállay, M.; Nagy, P. R.; Mester, D.; Rolik, Z.; Samu, G.; Csontos, J.; Csóka, J.; Szabó, P. B.; Gyevi-Nagy, L.; Hégely, B.; Ladjánszki, I.; Szegedy, L.; Ladóczki, B.; Petrov, K.; Farkas, M.; Mezei, P. D.; Ganyecz, Á. *MRCC*, a quantum chemical program suite, https://www.mrcc.hu (accessed July 6, 2022).
(20) Matthews, D. A.; Cheng, L.; Harding, M. E.; Lipparini, F.; Stopkowicz, S.; Jagau, T. -C.; Szalay, P. G.; Gauss, J.; Stanton, J. F. Coupled-Cluster Techniques for Computational Chemistry: the CFOUR Program Package. *J. Chem. Phys.* **2020**, *152*, 214108.
(21) Stanton, J. F.; Gauss, J.; Cheng, L.; Harding, M. E.; Matthews, D. A.; Szalay, P. G; Auer, A. A.; Bartlett, R. J.; Benedikt, U.; Berger, C., et al. *CFOUR*, a quantum chemical program package, http://www.cfour.de (accessed July 6, 2022).
(22) Rey, M.; Nikitin, A. V.; Tyuterev, Vl. G. Ab initio ro-vibrational Hamiltonian in irreducible tensor formalism: a method for computing energy levels from potential energy surfaces for symmetric-top molecules. *Molecular Physics*. **2010**, *108*, 2121–2135.
(23) Rey, M.; Nikitin, A. V.; Tyuterev, V. G. Complete nuclear motion Hamiltonian in the irreducible normal mode tensor operator formalism for the methane molecule. *J. Chem. Phys.* **2012**, *136*, 244106.
(24) Rey, M. Group-theoretical formulation of an Eckartframe kinetic energy operator in curvilinear coordinates for polyatomic molecules. *J. Chem. Phys.* **2019**, *151*, 024101.
(25) Delahaye, T.; Nikitin, A.; Michaël, R.; Szalay, P. G.; Tyuterev, Vl. G. A new accurate ground-state potential energy surface of ethylene and predictions for rotational and vibrational energy levels. *J. Chem. Phys.* **2014**, *141*, 104301.
(26) Delahaye, T.; Nikitin, A.; Michaël, R.; Szalay, P. G.; Tyuterev, Vl. G. Accurate 12D dipole moment surfaces of ethylene. *Chem. Phys. Lett.* **2015**, *639*, 275–282.
(27) Rey, M.; Nikitin, A.; Campargue, A.; Kassi, S.; Mondelain, D.; Tyuterev, V. Ab initio variational predictions for understanding highly congested spectra: rovibrational assignment of 108 new methane sub-bands in the icosad range (6280–7800 cm^{-1}). *Phys. Chem. Chem. Phys.* **2016**, *18*, 176–189.
(28) Rey, M.; Nikitin, A. V.; Babikov, Y. L.; Tyuterev, V. G. TheoReTS – An information system for theoretical spectra based on variational predictions from molecular potential energy and dipole moment surfaces. *J. Mol. Spectrosc.* **2016**, *327*, 138–158.
(29) Rey, M.; Nikitin, A.V., Tyuterev, V. G. Accurate Theoretical Methane Line Lists in the Infrared up to 3000 K and Quasi-continuum Absorption/Emission Modeling for Astrophysical Applications. *The Astrophysical Journal* **2017**, *847*, 105.
(30) Rey, M.; Chizhmakova, I. S.; Nikitin, A. V.; Tyuterev, V. G. Understanding global infrared opacity and hot bands of greenhouse molecules with low vibrational modes from first-principles calculations: the case of CF_4. *Phys. Chem. Chem. Phys.* **2018**, *20*, 21008.
(31) Viglaska, D.; Rey, M.; Nikitin, A. V.; Tyuterev, V. G. Isotopic and symmetry breaking effects on phosphine spectra under H → D substitutions from ab initio variational calculations. *J. Chem. Phys.* **2018**, *149*, 174305.
(32) Egorov, O.; Nikitin, A.; Rey, M.; Rodina, A.; Tashkun, S.; Tyuterev, V. Global modeling of NF_3 line positions and intensities from far to mid-infrared up to 2200 cm^{-1}. *J. Quant. Spectrosc. Radiat. Transfer* **2019**, *239*, 106668.
(33) Viglaska-Aflalo, D.; Rey, M.; Nikitin, A.; Delahay, T. A global view of isotopic effects on ro-vibrational spectra of six-atomic molecules: a case study of eleven ethylene species. *Phys. Chem. Chem. Phys.* **2020**, *22*, 3204–3216.

(34) Rey, M.; Chizhmakova, I. S.; Nikitin, A. V.; Tyuterev, V. G. Towards a complete elucidation of the ro-vibrational band structure in the SF_6 infrared spectrum from full quantum-mechanical calculations. *Phys. Chem. Chem. Phys.* **2021**, *23*, 12115–12126.
(35) Egorov, O.; Rey, M.; Nikitin, A.; Viglaska, D. New Ab Initio Potential Energy Surfaces for NH_3 Constructed from Explicitly Correlated Coupled-Cluster Methods. *J. Phys. Chem. A*, 2021, **125**, 10568–10579.
(36) Hougen, J. T.; Bunker, P. R.; Johns, J. W. C. The vibration-rotation problem in triatomic molecules allowing for a large-amplitude bending vibration. *J. Mol. Spectrosc.* **1970**, *34*, 136–172.
(37) Viglaska, D.; Rey, M.; Nikitin, A. V.; Tyuterev, V. G. Derivation of ρ-dependent coordinate transformations for nonrigid molecules in the Hougen–Bunker–Johns formalism. *J. Chem. Phys.* **2020**, *153*, 084102.
(38) Weil, J. A.; Howarth, D. F. Magnetic resonance spectroscopy of extra-terrestrial methyl radical. *Can. J. Phys*. **2009**, *87*, 709–719.
(39) Herzberg, G.; Shoosmith, J. Absorption spectrum of free CH_3 and CD_3 radicals. *Can. J. Phys*. **1956**, *34*, 523–525.
(40) Herzberg, G. The Spectra and Structures of Free Methyl and Free Methylene. *Proc. R. Soc. London A.* **1961**, *262(1310)*, 291–317.
(41) Callear, A. B.; Metcalfe, M. P. Oscillator strengths of the bands of the $\tilde{B}2A'1$—$\tilde{X}2A''2$ system of CD_3 and a spectroscopic measurement of the recombination rate comparison with CH_3. *Chem. Phys*. **1976**, *14*, 275.
(42) Westre, S. G.; Kelly, P. B.; Zhang, Y. P.; Ziegler, L. D. Subpicosecond predissociation dynamics of the methyl radical Rydberg 3s state. *J. Chem. Phys*. **1991**, *94*, 270.
(43) Westre, S. G.; Gansberg, T. E.; Kelly, P. B.; Ziegler, L. D. Structure and dynamics of higher vibronic levels in the methyl radical Rydberg 3s state. *J. Phys. Chem*. **1992**, *96*, 3610–3615.
(44) Settersten, T. B.; R. L. Farrow and J. A. Gray, Coherent infrared–ultraviolet double-resonance spectroscopy of CH_3. *Chem. Phys. Lett.* **2003**, *370*, 204–210.
(45) Wu, G.; Jiang, B.; Ran, Q.; Zhang, J.; Harich, S. A.; Yanga, X. Photodissociation dynamics of the methyl radical at 212.5 nm: Effect of parent internal excitation. *J. Chem. Phys*. **2004**, *120*, 2193.
(46) North, S. W.; Blank, D. A.; Chu, P. M.; Lee, Y. T. Photodissociation dynamics of the methyl radical 3s Rydberg state. *J. Chem. Phys*. **1995**, *102*, 792.
(47) Yu, H. T.; Sevin, A.; Kassab, E.; Evleth, E. M. A comparative theoretical analysis of the photochemistry of the methyl radical and related systems. *J. Chem. Phys*. **1984**, *80*, 2049.
(48) Zanchet, A.; Bañares, L.; Senentc, M. L.; García-Vela, A. Ab initio study of the ground and excited electronic states of the methyl radical. *Phys. Chem. Chem. Phys*. **2016**, *18*, 33195–33203.
(49) García-Vela, A. Photodissociation of the methyl radical: the role of nonadiabatic couplings in enhancing the variety of dissociation mechanisms. *Phys. Chem. Chem. Phys*. **2021**, *23*, 25911–25924.
(50) Botschwina, P.; Schick, E.; Horn, M. The barrier to dissociation in the $\tilde{B}2A1$' state of the methyl radical. *J. Chem. Phys*. **1993**, *98*, 9215.
(51) Mebel, A. M.; Lin, S. -H. Excited electronic states of the methyl radical. Ab initio molecular orbital study of geometries, excitation energies and vibronic spectra. *Chem. Phys.* **1997**, *215*, 329–341.
(52) Loos, P. -F.; Scemama, A.; Boggio-Pasqua, M.; Jacquemin, D. Mountaineering Strategy to Excited States: Highly Accurate Energies and Benchmarks for Exotic Molecules and Radicals. *J. Chem. Theory Comput*. **2020**, *16*, 3720–3736.
(53) DiGiuseppe, T. G.; Hudgens, J. W.; Lin, M. C. Multiphoton ionization of methyl radicals in the gas phase. *J. Phys. Chem*. **1982**, *86*, 36–41.
(54) DiGiuseppe, T. G.; Hudgens, J. W.; Lin, M. C. New electronic states in CH_3, observed using multiphoton ionization. *J. Chem. Phys*. **1982**, *76*, 3337.
(55) Hudgens, J. W.; DiGiuseppe, T. G.; Lin, M. C. Two photon resonance enhanced multiphoton ionization spectroscopy and state assignments of the methyl radical. *J. Chem. Phys*. **1983**, *79*, 571.
(56) Heinze, J.; Heberle, N.; Kohse-Höinghaus, K. The CH_3 $3p_z\ ^2A_2'' \leftarrow \tilde{X}\ ^2A_2''\ 0_0^0$ band at temperatures up to 1700 K investigated by REMPI spectroscopy. *Chem. Phys. Lett*. **1994**, *223*, 305–312.
(57) Zhang, B.; Zhang, J.; Liu, K. Imaging the "missing" bands in the resonance-enhanced multiphoton ionization detection of methyl radical. *J. Chem. Phys*. **2005**, *122*, 104310.
(58) Fu, H. B.; Hu, Y. J.; Bernstein, E. R. IR/UV double resonant spectroscopy of the methyl radical: Determination of in the Rydberg state. *J. Chem. Phys*. **2005**, *123*, 234307.
(59) Zhang, W.; Kawamata, H.; Merer, A. J.; Liu, K. IR−UV Double-Resonance of Methyl Radicals and a Determination of the Detection Sensitivity of REMPI Bands. *J. Phys. Chem. A*. **2009**, *113*, 13133–13138.
(60) Wu, Y.; Bottom, A.; Zhang, Z.; Ombrello, T. M.; Katta, V. R. Direct measurement of methyl radicals in a methane/air flame at atmospheric pressure by radar REMPI. *Optics Express*. **2011**, *19*, 23997–24004.

(61) Pan, H.; Liu, K. Imaging spectroscopy of the missing REMPI bands of methyl radicals: Final touches on all vibrational frequencies of the 3p Rydberg states. *J. Chem. Phys*. **2018**, *148*, 014303.
(62) Black, J. F.; Powis, I. Rotational structure and predissociation dynamics of the methyl 4pz(v=0) Rydberg state investigated by resonance enhanced multiphoton ionization spectroscopy. *J. Chem. Phys*. **1988**, *89*, 3986.
(63) Grzesiak, J.; Vashishta, M.; Djuricanin, P.; Stienkemeier, F.; Mudrich, M.; Dulitz, K.; Momose, T. Production of rotationally cold methyl radicals in pulsed supersonic beams. *Rev. Sci. Instrum*. **2018**, *89*, 113103.
(64) Milligan, D. E.; Jacox, M. E. Infrared and Ultraviolet Spectroscopic Study of the Products of the Vacuum-Ultraviolet Photolysis of Methane in Ar and N_2 Matrices. The Infrared Spectrum of the Free Radical CH_3. *J. Chem. Phys*. **1967**, *47*, 5146.
(65) Snelson, A. Infrared matrix isolation spectrum of the methyl radical produced by pyrolysis of methyl iodide and dimethyl mercury. *J. Phys. Chem*. **1970**, *74*, 537–544.
(66) Jacox, M. E. Matrix isolation study of the infrared spectrum and structure of the CH_3 free radical. *J. Mol. Spectrosc*. **1977**, *66*, 272–287.
(67) Tan, L. Y.; Winer, A. M.; Pimentel, G. C. Infrared Spectrum of Gaseous Methyl Radical by Rapid Scan Spectroscopy. *J. Chem. Phys*. **1972**, *57*, 4028.
(68) Yamada, C.; Hirota, E.; Kawaguchi, K. Diode laser study of the ν_2 band of the methyl radical. *J. Chem. Phys*. **1981**, *75*, 5256.
(69) Holt, P. L.; McCurdy, K. E.; Weisman, R. B.; Adams, J. S.; Engel, P. S. Transient CARS spectroscopy of the ν_1 band of methyl radical. *J. Chem. Phys*. **1984**, *81*, 3349.
(70) Triggs, N. E.; Zahedi, M.; Nibler, J. W.; DeBarber, P.; Valentini, J. J. High resolution study of the v1 vibration of CH_3 by coherent Raman photofragment spectroscopy. *J. Chem. Phys*. **1992**, *96*, 1822.
(71) Zahedi, M.; Harrison, J. A.; Nibler, J. W. 266 nm CH_3I photodissociation: CH_3 spectra and population distributions by coherent Raman spectroscopy. *J. Chem. Phys*. **1994**, *100*, 4043.
(72) Kelly, P. B.; Westre, S. G. Resonance Raman spectroscopy of the methyl radical. *Chem. Phys. Lett*. **1998**, *151*, 253–257.
(73) Amatatsu, Y.; Morokuma, K.; Yabushita, S. Ab initio potential energy surfaces and trajectory studies of A-band photodissociation dynamics: $CH_3I^* \rightarrow CH_3+I$ and CH_3+I^*. *J. Chem. Phys*. **1991**, *94*, 4858.
(74) Amano, T.; Bernath, P. F.; Yamada, C.; Endo, Y.; Hirota, E. Difference frequency laser spectroscopy of the ν_3 band of the CH_3 radical. *J. Chem. Phys*. **1982**, *77*, 5284.
(75) Davis, S.; Anderson, D. T.; Duxbury, G.; Nesbitt, D. J. Jet-cooled molecular radicals in slit supersonic discharges: Sub-Doppler infrared studies of methyl radical. *J. Chem. Phys*. **1997**, *107*, 5661.
(76) Pacansky, J.; Bargon, J. Low temperature photochemical studies on acetyl benzoyl peroxide. Observation of methyl and phenyl radicals by matrix isolation infrared spectroscopy. *J. Am. Chem. Soc*. **1975**, *97*, 6896–6897.
(77) Jacox, M. E. Vibrational and Electronic Energy Levels of Polyatomic Transient Molecules. Supplement B. *J. Phys. Chem. Ref. Data*. **2003**, *32*, 1–441.
(78) Hoshina, H.; Fushitani, M.; Momose, T. Infrared spectroscopy of rovibrational transitions of methyl radicals (CH_3, CD_3) in solid parahydrogen. *J. Mol. Spectrosc*. **2011**, *268*, 164–172.
(79) Yamada, C.; Hirota, E. The transition dipole moment of the ν_2 band of the methyl radical. *J. Chem. Phys*. **1983**, *78*, 669.
(80) Wormhoudt, J.; McCurdy, K. E. A measurement of the strength of the ν_2 band of CH_3. *Chem. Phys. Lett*. **1989**, *156*, 47–50.
(81) Stancu, G. D.; Röpcke, J.; Davies, P. B. Line strengths and transition dipole moment of the ν_2 fundamental band of the methyl. *J. Chem. Phys*. **2005**, *122*, 014306.
(82) Botschwina, P.; Flesch, J.; Meyer, W. Spectroscopic properties of the methyl radical calculated from UHF SCEP wavefunctions. *Chem. Phys*. **1983**, *74*, 321–338.
(83) Tanarro, I.; Sanz, M. M; Bermejo, D.; Domingo, C.; Santos, J. Double modulation-high resolution infrared spectroscopic technique: The ν_3 band of the CH_3 radical and excited states of CH_4 in a hollow cathode discharge. *J. Chem. Phys*. **1994**, *100*, 238.
(84) Tanarro, I.; Sanz, M. M.; Domingo, C.; Bermejo, D.; Santos, J.; Domenech, J. L. Transition dipole moment of the ν_3 band of CH_3. *J. Phys. Chem.* **1994**, *98*, 5862–5866.
(85) Bethardy, G. A.; Glen Macdonald, R. Direct measurement of the transition dipole moment of the ν_3 asymmetric C–H stretching vibration of the CH_3 radical. *J. Chem. Phys*. **1995**, *103*, 2863.

(86) Stancu, G. D.; Röpcke, J.; Davies, P. B. Measurement of the transition dipole moment of the first hot band of the v_2 mode of the methyl radical by diode laser spectroscopy. *J. Phys. Chem. A.* **2008**, *112*, 6285–6288.
(87) Rey, M. Novel methodology for systematically constructing global effective models from ab initio-based surfaces: A new insight into high-resolution molecular spectra analysis. *J. Chem. Phys.* **2022**, *156*, 224103.
(88) Bunker, P. R; Jensen, P. *Molecular Symmetry and Spectroscopy*; NRC Research Press, Ottawa, 2012.
(89) Papoušek, D.; Aliev, M. R. *Molecular Vibrational-Rotational Spectra. Theory and Applications of High Resolution Infrared, Microwave and Raman Spectroscopy of Polyatomic Molecules*; Elsevier Scientific Pub. Co: Amsterdam, Oxford, New York, 1982.
(90) Knowles, P. J.; Hampel, C.; Werner, H. -J. Coupled cluster theory for high spin, open shell reference wave functions. *J. Chem. Phys.* **1993**, *99*, 5219.
(91) Knowles, P. J.; Hampel, C.; Werner, H. -J. Erratum: "Coupled cluster theory for high spin, open shell reference wave functions" [J. Chem. Phys. 99, 5219 (1993)]. *J. Chem. Phys.* **2000**, *112*, 3106.
(92) Lee, T. J.; Taylor, P. R. A diagnostic for determining the quality of single-reference electron correlation methods. *Int. J. Quant. Chem.* **1989**, *36*, 199–207.
(93) Janssen, C. L.; Nielsen, I. M. B. New diagnostics for coupled-cluster and Møller–Plesset perturbation theory. *Chem. Phys. Lett*. **1998**, *290*, 423–430.
(94) Dunning, T. H. Gaussian basis sets for use in correlated molecular calculations. I. The atoms boron through neon and hydrogen. *J. Chem. Phys.* **1989**, *90*, 1007.
(95) Peterson, K. A.; Woon, D. E.; Dunning, T. H. Benchmark calculations with correlated molecular wave functions. IV. The classical barrier height of the H+H2→H2+H reaction. *J. Chem. Phys.* **1994**, *100*, 7410.
(96) Knizia, G.; Adler, T. B.; Werner, H. -J. Simplified CCSD(T)-F12 methods: Theory and benchmarks. *J. Chem. Phys.* **2009**, *130*, 054104.
(97) Hill, J. G.; Mazumder, S.; Peterson, K. A. Correlation consistent basis sets for molecular core-valence effects with explicitly correlated wave functions: The atoms B–Ne and Al–Ar. *J. Chem. Phys*. **2010**, *132*, 054108.
(98) J. Gauss, A. Tajti, M. Kállay, J. F. Stanton and P. G. Szalay, *J. Chem. Phys.*, 2006, **125**, 144111.
(99) Nikitin. A. V.; Rey, M.; Tyuterev, Vl. G. First fully ab initio potential energy surface of methane with a spectroscopic accuracy. *J. Chem. Phys.* **2016**, *145*, 114309.
(100) Nikitin, A. V.; Protasevich, A. E.; Rodina, A. A.; Rey, M.; Tajti, A.; Tyuterev, V. G. Vibrational levels of formaldehyde: Calculations from new high precision potential energy surfaces and comparison with experimental band origins. *J. Quant. Spectrosc. Radiat. Transfer*. **2021**, *260*, 107478.
(101) Hirota, E.; Yamada, C. Intramolecular motions and molecular structure of the CH_3 radical. *J. Mol. Spectrosc*. **1982**, *96*, 175–182.
(102) Špirko, V.; Bunker, P. R. The Potential Function and Rotation-Vibration Energy Levels of the Methyl Radical CH_3. *J. Mol. Spectrosc*. **1982**, *95*, 381–390.
(103) Šimečková, M.; Jacquemart, D.; Rothman, L. S.; Gamache, R. R.; Goldman, A. Einstein A-coefficients and statistical weights for molecular absorption transitions in the HITRAN database. *J. Quant. Spectrosc. Radiat. Transfer*. **2006**, *98*, 130–155.

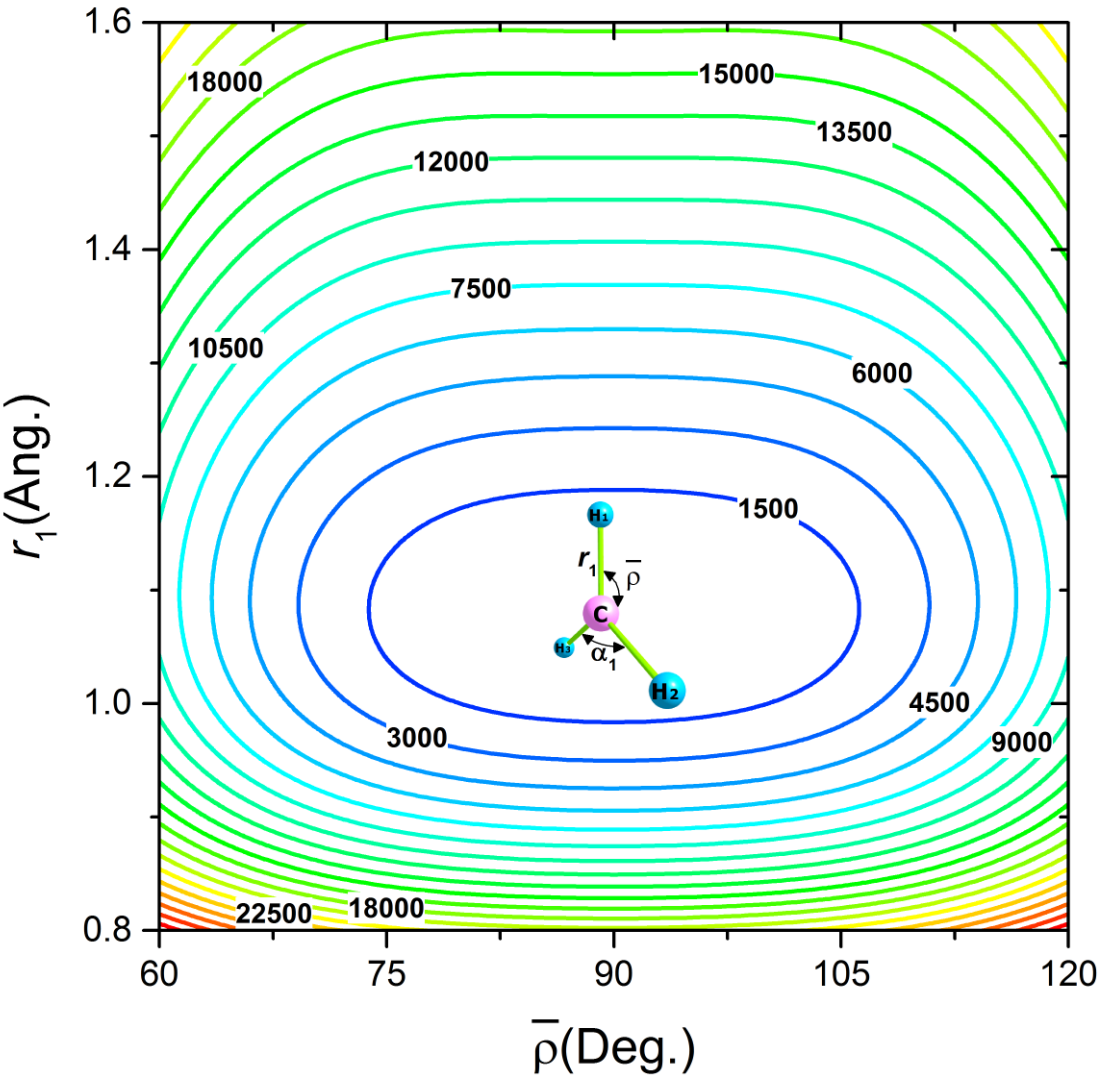
1.6
1.4
1.2
1.0
0.8
60
75
90
105
120
r_1(Ang.)
$\bar{\rho}$(Deg.)
18000
15000
13500
12000
7500
10500
6000
1500
4500
9000
3000
22500
18000
H1
H2
H3
C
r_1
$\bar{\rho}$
α_1

TOC graphic